Investigation of the Impact of Urbanization to Urban Heat Island – A Comparison Between Perth and Muscat

Qais Al-Badi [1], Petra Helmholz[1], Dimitri Bulatov[2]

[1] School for Earth and Planetary Sciences, Curtin University, Kent Street, Bentley, Australia, q.al-badi@student.curtin.edu.au, petra.helmholz@curtin.edu.au

[2] Fraunhofer IOSB, Ettlingen, Germany - dimitri.bulatov@iosb.fraunhofer.de

Keywords: Surface Urban Heat Island, Land Surface Temperature, MODIS, Landsat, Muscat, Perth

ABSTRACT

Urbanization has led to changes in land use and land cover (LU/LC) from non-urban areas to urban areas, significantly impacting local climates, particularly through the Surface Urban Heat Island (SUHI) effect, where urban areas are warmer than rural ones. This study quantifies the impact of urbanization on SUHI intensity in Perth and Muscat, analysing how LU/LC changes influence SUHI intensity and its spatio-temporal patterns. Utilizing high-resolution Landsat 8 and Landsat 7/5 data, along with MODIS's temporal capabilities, the research provides an in-depth understanding of LU/LC changes and their implications on SUHI dynamics. For analysing LU/LC changes, data processing involved cloud-pixel elimination, atmospheric correction, and Co-registration of MODIS and Landsat. Land surface temperature (LST) is derived from Landsat imagery by calculating radiance, brightness temperature, and emissivity, followed by correction for land cover type. The research findings demonstrate the significant impact of urban expansion on local climates and the strong influence of LU/LC patterns on SUHI intensity in Perth and Muscat.

1. Introduction

The study of Urban Heat Islands (UHIs) has been a subject of scientific investigation for over four decades. Oke (1982) defined the concept as urban environments that experience warmer temperatures than their rural surroundings. Urbanization, population growth, and industrialization lead to increases in temperature, and this situation adversely affects the world, especially in urban areas (Aslan & Koc-San, 2021).

Transformations in urban thermal characteristics carry significant implications for urban sustainability by altering local climate patterns, including precipitation and summertime temperature extremes. These changes contribute to increased health risks, resource scarcity, and pollution capture, posing major challenges for sustainable urban development (Dutta et al., 2019). Zhang et al. (2009) report that in urban areas, heatstroke diseases tend to rise while (Grimmond, 2007) mentions risks for the natural environment affecting urban biological diversity and water status. It highlights that UHI must be understood. As urban areas continue to expand, understanding the relationship between land use/land cover (LU/LC) changes, such as the increase of urban settlement and reduction in vegetation cover, and LST patterns is crucial (Dutta et al., 2019).

Unlike the traditional UHI, which primarily considers air temperature differences between urban and rural areas, surface urban heat islands (SUHI) focus on Land Surface Temperature (LST) variations, which can be derived from remotely sensed images reflecting the actual temperature of the urban environment's physical surfaces (Dutta et al., 2019) arises from complex interactions between urban development and environmental factors. The phenomenon is primarily driven by replacing natural, heat-absorbing surfaces with impervious, heat-retaining materials like asphalt and concrete (Santamouris, 2015).

The recognition and study of SUHI have become an essential part of urban climate change assessment. This research centers on investigating the SUHI effects in Perth, Australia, and Muscat, Oman (Figure 1). The selection of these cities is based on distinct criteria, considering geographical location, climatic conditions, urban development, and data availability.

Perth, located in Australia's southwestern part, has a Mediterranean climate and exhibits moderate temperatures, distinct wet and dry seasons, and mild winters. Perth has had substantial urban development in recent years. The city is marked by a mix of land uses, significant suburban expansion, and a rich presence of green spaces and water bodies. This unique combination makes Perth a key example for studying SUHI dynamics (City of Perth, 2015, Bulatov et al., 2020).

The second test site, Muscat, Oman's capital city, is located on the Arabian Peninsula, has a slightly more arid climate than Perth while also facing scorching temperatures in its hot desert climate, especially during summer, often exceeding 40°C (104°F). Similarly to Perth, Muscat experienced rapid urbanization. The city's urban landscape, characterized by high-density housing, commercial buildings, and limited greenery, provides a unique perspective on the SUHI effects in arid environments (Nebel & von Richthofen, 2016).

Figure 1: Satellite images of Perth Metropolitan Area (left) and Muscat (right) by Google.

Both cities share proximity to the sea, which influences their climates and exacerbates SUHI effects due to the interaction between urban heat and maritime air masses, leading to intensified SUHI phenomena.

The study will address key questions including identifying significant land use and land cover changes observed in these cities, exploring the correlation between these changes and variations in SUHI intensity, and examining how the intensity and spatial distribution of SUHI have varied in Perth and Muscat

during 2000 and 2020. Firstly, we focus on identifying and quantifying the changes in LU/LC in Perth and Muscat over the last two decades and examining their correlation with urban growth. Utilizing supervised classification, the study will categorize land cover types into urban areas (residential, commercial, and mixed-use developments), industrial zones (factories, warehouses), vegetation areas (parks, gardens, natural vegetation), water bodies (rivers, lakes, coastal areas), and bare soil (undeveloped or transitional lands). Secondly, we investigate the correlation between LU/LC changes and variations in SUHI intensity in Perth and Muscat, with a particular focus on areas of urbanization identified previously. This objective aims to explore the interrelationship between LU/LC transformations and SUHI, determining how these changes influence SUHI's distribution and intensity in both cities. Finally, this research delves into understanding how the intensity and spatial distribution SUHI vary in Perth and Muscat. The primary aim is to conduct a temporal analysis of SUHI development, tracking and analysing changes in SUHI intensity over time to gain insights into the evolution of urban heat islands in relation to urban development patterns.

This paper is structured as follows: After a literature review in Section 2, the data and methodology are introduced in Sections 3 and 4. The validation of the LU/LC and LST accuracy is presented in Section 5. The Land Use/Land Cover Changes and SUHI Intensity analysis is presented in Section 6 and the paper closes with a discussion and conclusion in Section 7.

2. Literature review

The main mechanism that causes SUHI is the amount of surface heating created by impervious material in a city, such as roads and buildings, which absorb and emit heat to a greater extent than most natural surfaces. On a warm day, conventional roofing materials may reach as high as 16°C/60°F warmer than air temperatures (Fallatah & Imam, 2023). The literature indicates a multifaceted relationship between LU/LC changes and SUHI dynamics. Different LU/LC types have different impacts on SUHI, depending on their albedo, emissivity, vegetation cover, imperviousness, and anthropogenic heat sources (Fallatah & Imam, 2023).

Vegetation cover plays a crucial role in influencing an area's cooling potential, which in turn affects the intensity of SUHI. This relationship can be quantified using multispectral sensors that capture the necessary data to calculate the Normalized Difference Vegetation Index (NDVI), which serves as an indicator of the level and health of vegetation; healthier, denser vegetation typically corresponds to a higher NDVI value and greater cooling effect, thereby mitigating SUHI intensity (Li et al., 2022).

Another factor is the Normal Difference Built-up Index (NDBI), a satellite-derived index that plays a crucial role in identifying and quantifying built-up areas that contribute to the SUHI effect by analyzing high-resolution satellite imagery and utilizing GIS. NDBI leverages the distinct reflectance values of urban materials across specific wavelengths to calculate the built-up area index (Morabito et al., 2021). This index is crucial in assessing how much of the urban landscape is covered by surfaces that retain heat and reduce water permeability, thereby intensifying the SUHI effects.

Shahfahad et al. (2022) examined the influence of LU/LC changes on SUHII in Delhi. Their approach using Landsat datasets and advanced statistical methods like geographically weighted regression (GWR) and urban thermal field variation index (UTFVI) resonates with the importance of remote sensing and GIS technologies. Their findings underscore the significant impact of urban expansion on local climate, highlighting the strong impact of LU/LC patterns on SUHII, as previously described. Similarly, Morabito et al. (2021) contribute to understanding the balance between built and green spaces in urban areas. Their study in Italian metropolitan cities, using a new urban surface landscape layer (USLAND), MODIS/Terra, and Sentinel data, highlights the crucial role of tree cover in mitigating SUHI effects, a point that complements the discussion on vegetation's cooling potential.

Liu et al. (2022) extend the discussion on urban expansion by investigating the effects of built-up area expansion in China. Using long-term space-borne observations of LST and land cover, they applied various methods to measure UBAE and UHI. Their findings about seasonal variations in UHI intensity provide a nuanced understanding of the temporal dynamics of SUHI, a topic touched upon in the initial sections. The study by Chen et al. (2022) on Wuhan's main urban area uses Landsat imagery to explore the relationship between land cover changes, green spaces, and UHI, further demonstrating the practical applications of remote sensing in urban climate studies, as advocated in earlier sections.

The implications of urbanization patterns and existing atmospheric conditions necessitate innovative land use planning and development strategies that can harmonize urban growth with ecological sustainability. Incorporating urban green spaces, optimizing building designs for thermal comfort, and enhancing urban albedo through reflective surfaces are some of the potential strategies that could mitigate the SUHI effects associated with these development patterns (Shastri & Ghosh, 2019).

To conclude: The occurrence and severity of SUHIs are determined by a combination of LST measurements, vegetation cover's cooling capacity, and the extent of built-up areas as indicated by NDBI. Each factor contributes uniquely to the understanding and mitigation of SUHI effects.

A comprehensive understanding of SUHI formation, the contributing factors, and the impacts of different land development styles is imperative for framing effective mitigation strategies and fostering urban sustainability. Remote sensing and GIS data are crucial components in studying and addressing the challenges posed by UHIs.

The distinct urbanization patterns in Perth and Muscat significantly impact the formation and intensity of SUHIs. Liu et al. (2022) highlighted the role of low-density housing and mixed retail/commercial development in intensifying SUHI effects. Perth is known for its expansion outward from the Swan River, which is characterized by various suburbs and a central business district, reflecting a mix of residential and commercial development. This contrasts sharply with the dense urban core of Muscat, known for its low-lying white buildings and a vibrant economy influenced by trade, petroleum, and porting. These distinct urban landscapes in Perth and Muscat contribute differently to their respective SUHI intensities due to the varied nature of urban development and land use.

3. Data

To accurately analyze SUHI in the selected study areas, Perth and Muscat, multi-source data was collected. The sources included satellite imagery, meteorological datasets, and Geographic Information System (GIS) data repositories to understand land

surface temperature, vegetation cover, and land use/land cover changes over the period 2000 to 2020. The selection of imagery at five-year intervals within this timeframe was crucial to observing significant urban and land cover changes that correlate with variations in (SUHI) intensity. This multifaceted approach ensures a thorough analysis of the various factors influencing SUHI in these distinct urban environments. For Perth and Muscat, the data was carefully chosen during the hottest months: December to February for Perth and June to August for Muscat.

Table 1 details the satellite images used for this paper. Since Landsat data have both spectral and thermal bands, this study used Landsat images to maintain data consistency. The different Landsat missions used for this study include 5, 7 ETM+, and 8 (OLI/TIRS). For Perth, the Path/Row was 113/082; for Muscat 158/044. All images have been sourced from USGS Earth Explorer (earthexplorer.usgs.gov/) and have a spatial resolution of 30 meters.

For the Landsat 7 ETM+ data affected by the "SLC-off" issue, Landsat 7 ETM+ imagery acquired after May 2003 was flawed due to a malfunction of the Scan Line Corrector. In each image, about 20% of pixels were lost. Landsat 5 images were selected for Perth for 2005 and 2010 to keep the data consistent. In the case of Muscat, where no alternative Landsat 5 data were available, the missing information in the Landsat 7 ETM+ images from 2005 and 2010 was filled in using the gap-fill function in QGIS. Finally, cloud masking was carried out with a specific plugin in QGIS, following the established procedure from Landsat's manual to remove the impact of clouds and shadows. This ensured that the extracted data accurately represented the surface conditions.

Landsat		**MODIS**	
Perth	*Muscat*	*Perth*	*Muscat*
20/02/2000 (Landsat 7 ETM+)	14/06/2000 (Landsat 5)	24/02/2000	14/06/2000
24/01/2005 (Landsat 5)	22/07/2005 (Landsat 7 ETM+)	26/01/2005	22/07/2005
22/01/2010 (Landsat 5)	24/08/2011 (Landsat 7 ETM+)	21/01/2010	24/08/2011
22/12/2015 Landsat 8 (OLI/TIRS))	10/07/2015 (Landsat 8 (OLI/TIRS))	22/12/2015	10/07/2015
19/12/2020 Landsat 8 (OLI/TIRS))	05/06/2020 (Landsat 8 (OLI/TIRS))	19/12/2020	05/06/2020

Table 1: Modis and Landsat data for Perth and Muscat used for the analysis of SUHI. The Landsat Path/Row for Perth 113/082; and for Muscat 158/044.

MODIS data shown in Table 1 was retrieved from *earthdata.nasa.gov* to provide a higher temporal (daily) and spatial resolution (1 km), guaranteeing consistent measurement parameters for comparative analysis over time and between the two cities, used for Validating Landsat LST.

In addition, the study incorporates temperature data from the Bureau of Meteorology for Perth and accesses records from 'Muscat Climate - Weather History - Oman' to enhance the correlation between satellite-derived LST and actual air temperatures. For LULC classification validating, Google Earth imagery and OSM data are utilized, offering detailed depictions of urban infrastructure, and aiding in identifying different development patterns within the cities of Perth and Muscat.

4. Methodology

The procedural methodology of this study is shown in Figure 2. In this section, each of the different steps are described in detail.

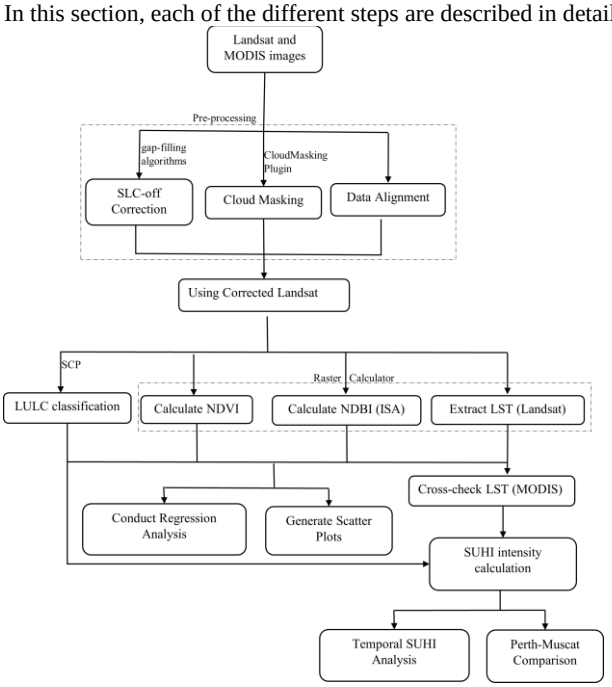

Figure 2: The flowchart of the overall processes.

4.1 Land Use and Land Cover Classification

Supervised classification (Maximum Likelihood Classification (MLC)) was employed to delineate various land cover classes within the study areas of Perth and Muscat. Representative training sites for each land cover class were identified. These sites were chosen based on observable characteristics within the images to discern the distinct features of each land cover class for accurate classification. The band combination of different bands in a sequence of RGB (Landsat 5/7: Natural color 321, Urban 753; Vegetation 432), (Landsat8: Natural color 432, Urban 764, Vegetation 543) helps distinguish different land surface features.

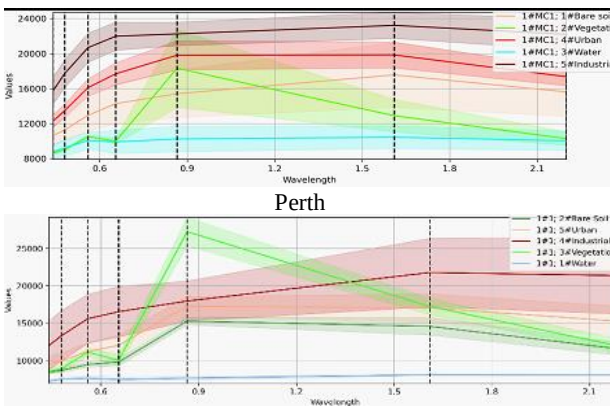

Figure 3: Spectral Signature Plot of Perth (top) and Muscat (bottom).

For each land cover class, spectral signatures were developed by delineating sample areas on the satellite images that accurately represented *water, industrial, urban, vegetation, and bare soil/rock* features (Table 2). Figure 3 shows Perth exhibits a higher reflectance in the near-infrared band (0.77-0.89 μm), indicative of its abundant vegetation. In contrast, Muscat,

characterized by arid conditions, presents a higher reflectance in the shortwave infrared bands (1.55-1.75 μm and 2.09-2.35 μm), suggesting the presence of *Bare Soil/Rocks*.

LULC classes	Description
Water	Areas representing bodies of water (rivers, lakes, and coastal zones).
Industrial	Regions containing manufacturing facilities, warehouses, and other industrial structures.
Urban	Residential and commercial areas, including mixed-use developments.
Vegetation	Parks, gardens, forests, and other forms of greenery.
Bare Soil	Unpaved, undeveloped land or areas undergoing transition, devoid of significant vegetation or built structures.

Table 2: Details of LULC Classes

The primary classification was refined through manual adjustments, rectifying misclassified regions using additional verified interpretation of high-resolution satellite images (Google Earth and existing maps and datasets.)

4.2 Indices Calculation: NDVI and NDBI (ISA)

The spectral indices NDVI and NDBI were central to analyzing land cover characteristics. These indices were derived the years 2000, 2005, 2010, 2015, and 2020. NDVI, highlighting vegetation, was computed from Landsat data using equation (1).

$$\text{NDVI} = \frac{\text{NIR} - \text{Red}}{\text{NIR} + \text{Red}} \quad (1)$$

where NIR represents the near-infrared band and Red is the visible red band, with band numbers varying between Landsat versions (Bands 4 and 3 for Landsat 5 and 7, and Bands 5 and 4 for Landsat 8).

Similarly, NDBI, indicating built-up areas, was computed using the same Landsat data using equation (2).

$$\text{NDBI} = \frac{\text{SWIR} - \text{NIR}}{\text{SWIR} + \text{NIR}} \quad (2)$$

where SWIR is the short-wave infrared band and NIR is the near-infrared band. Bands 5 and 4 were used for Landsat 5 and 7, respectively, and Bands 6 and 5 were used for Landsat 8. The NDBI exhibits values between -1 and +1. As the NDBI increases, it indicates more urbanized or built-up areas, signifying more extensive construction land coverage.

Additionally, the built-up area was estimated by combining NDBI and NDVI values to minimize spectral confusion between *bare land* and *urban areas*, as both exhibit similar characteristics in the NIR band. This method's effectiveness was enhanced by its sensitivity to chlorophyll through NDVI using equation (3) allowing to obtain the built-up area (BuA).

$$\text{BuA} = \text{NDBI} - \text{NDVI} \quad (3)$$

The final step involved classifying the resultant NDVI and NDBI into respective land cover categories based on specific threshold values of index ranges. These calculated indices proved essential for subsequent analysis steps, offering quantitative measures of vegetation cover and urban extent necessary for the study.

4.3 Extraction and Analysis of Land Surface Temperature (LST)

Creating LST maps from Landsat imagery involves several steps, each employing satellite data attributes and conversion factors. The Landsat-derived LST maps are validated against the MODIS LST data product "MOD11A1" to ensure accuracy.

For Landsat 8, the spectral radiance for Band (10) was calculated using the radiance scaling factors from the metadata (M_L and A_L) as shown in equation (4) and (5).

$$Radiance = (M_L \times Q_{band10}) + A_L \quad (4)$$

$$Radiance = (M_L \times Q_{band11}) + A_L \quad (5)$$

M_L and A_L are the multiplicative and additive rescaling factors, respectively, provided in the Landsat 8 metadata file, while $Q_{band10,11}$ is the digital number value for each band. These factors ensure that the raw *DN* values are accurately translated into physical measures of radiance reflecting the detected energy.

For Landsat 7/5, which include the Thematic Mapper (TM) and Enhanced Thematic Mapper Plus (ETM+) sensors, respectively, spectral radiance for thermal Band 6 is calculated differently using equation (6).

$$L_{\acute{\lambda}} = (LMAX_{\acute{\lambda}} - LMIN_{\acute{\lambda}}) \times Q + LMIN_{\acute{\lambda}} \quad (6)$$

The $LMAX_{\acute{\lambda}}$ and $LMIN_{\acute{\lambda}}$ are the maximum and minimum spectral radiance scaling constants obtained from the metadata for each band, while *Q* represent quantized calibrated pixel value linearly scaled between the minimum and maximum into the range [0;1]. This equation adjusts the *DN* values to account for the specific calibration of the satellite's thermal sensors, facilitating the comparison of thermal data over time and across different Landsat sensors.

The top of atmosphere brightness temperature (*T*) was then calculated using equation (7) whereby the conversion constants (*K1* and *K2*) are shown in Table 3.

$$T = K2 \,/\ln\left(\frac{K1}{L_{\acute{\lambda}}} + 1\right) \quad (7)$$

Sensor	Constant K1 (Watts/(m² * sr * μm))	Constant K2 (Kelvin)
Landsat 8 (Band 10)	774.89	1321.08
Landsat 8 (Band 11)	480.89	1201.14
Landsat 7 ETM+	666.09	1282.71
Landsat 5 TM	607.76	1260.56
Landsat 4 TM	671.62	1284.3

Table 3: Thermal Band Calibration Constants for Landsat Sensors.

The temperature *T* is then converted to LST using emissivity correction methods that account for land cover type—estimating the emissivity (ε) from the NDVI values calculated using a simple linear relationship using equation (8).

$$\varepsilon = a + b \times \text{NDVI} \quad (8)$$

where *a* and *b* are coefficients (0.986 and 0.004, respectively). Finally, we calculate the LST using equation (9).

$$LST = \frac{T_{B10}+T_{B11}}{2} / \left(1 + \lambda_{B10} \times \frac{T_{B10}}{\rho} \times \ln \varepsilon\right) \quad (9)$$

T_{B10} and T_{B11} are the brightness temperatures for Bands 10 and 11, λ_{B10} is the central wavelength of Band 10 (approximately

10.8μm), ρ is a constant incorporating Planck's constant, the speed of light, and the Stefan-Boltzmann constant (calculated as 2.384×10^{7}). The Landsat-derived LST maps were statistically and visually compared with the MODIS LST data to validate the accuracy of the Landsat LST. The statistical comparison involved calculating Mean Average Error (MAE) and Root Mean Square Error (RMSE).

4.4 UHI Intensity Calculation and Bi-Temporal Analysis

SUHI intensity underscores the difference in LST between urban and rural areas. To grasp SUHI evolution, a bitemporal analysis will contrast SUHI intensities at two distinct time points.

For SUHI calculation, the LU/LC urban and industrial areas are grouped as *'Urban'* while vegetable, water, and bare soil are considered *'Rural'*. This segregation is pivotal for accurately assessing the differential heat properties of these distinct land covers. Next, the average LST for the Urban and Rural areas are calculated. This was achieved by overlaying the LST data with LULC classifications, extracting the average LSTs for the Urban (merging Urban and Industrial) and Rural (merging Vegetation, Water, and Bare Soil) zones, ensuring accuracy in my analysis. Finally, SUHI Intensity was calculated by subtracting the average LST of the Rural areas from that of the Urban areas. SUHI is characterized as the difference in the LST of the urban pixels and the non-urban pixels (Karimi et al. 2021) using equation (10).

$$\mathrm{SUHI} = \mathrm{LST}_{\mathrm{Urban}} - \mathrm{LST}_{\mathrm{non-urban}} \quad (10)$$

The bi-temporal analysis involves a change detection assessment on urban land cover between two time points, pinpointing significant urban sprawl. This is cross-examined with shifts in SUHI intensity to understand their interplay. Preliminary results are poised to spotlight vulnerable regions in Perth and Muscat, particularly those with recent urban growth, in terms of SUHI susceptibility.

5. Validation

5.1 LULC Accuracy Assessment

The LULC classifications were subjected to a rigorous accuracy assessment to ensure their quality and practical utility. Employing Google satellite imagery as the reference data, error matrices were constructed utilizing test pixels. Congalton (1991) recommended that at least 50 test samples were systematically collected for each LULC class to facilitate a robust evaluation. If the area is large, at least 75 or 100 samples per class need to be used. This comprehensive approach enabled a thorough quantitative and qualitative classification accuracy assessment, thereby bolstering the confidence in the derived LULC maps. Therefore, more than 500 testing pixels per class were collected in this study. In Table 4, the overall accuracies were calculated above 95% for the 5 time periods between 2000 and 2020. Values below 90% are highlighted.

5.2 LST accuracy assessment

Table 5 presents a comparative analysis of LST data obtained from Landsat and MODIS satellites. The higher MAE and RMSE values suggest larger discrepancies and lower accuracy between Landsat and MODIS temperatures. These discrepancies could be attributed to several factors, including differences in spatial resolution, retrieval algorithms, and temporal sampling between Landsat and MODIS datasets. The difference in spatial resolution, with Landsat having a finer resolution of 30 meters compared to MODIS's coarser resolution of 1 km, is particularly significant and can lead to spatial averaging and loss of detail in MODIS data.

However, all calculated Correlation Coefficient (r) values are close to 1, indicating a strong positive linear relationship between the LST values of MODIS and Landsat in both cities across all time points. This shows that when the LST values in MODIS increase, the LST values in Landsat tend to increase as well, and vice versa, highlighting a general agreement in the data trends even with discrepancies in magnitude.

Perth		**2020**	**2015**	**2011**	**2005**
Water	**PA**	98.50	97.00	95.00	96.00
	UA	97.00	95.50	93.00	94.00
Bare soil	**PA**	98.00	97.80	98.00	97.00
	UA	98.50	98.00	97.50	96.50
Urban	**PA**	99.20	98.50	96.00	94.50
	UA	98.80	97.00	95.00	93.50
Vege-tation	**PA**	95.00	94.00	90.00	92.00
	UA	90.00	92.00	88.00	89.00
Indust-rial	**PA**	96.00	94.50	92.00	91.00
	UA	92.00	95.00	93.00	90.00
	Overall, Acc. %	97.50	96.60	95.50	94.80
Muscat		**2020**	**2015**	**2011**	**2005**
Water	**PA**	100.00	100.00	96.90	99.38
	UA	100.00	100.00	95.07	95.18
Bare soil	**PA**	99.86	99.65	99.30	99.08
	UA	99.86	99.96	98.37	99.20
Urban	**PA**	98.85	99.09	83.88	86.47
	UA	100.00	93.52	91.90	88.99
Vege-tation	**PA**	98.81	96.88	88.91	93.36
	UA	89.00	97.98	94.79	86.59
Indust-rial	**PA**	97.65	93.66	80.83	86.96
	UA	91.14	99.83	99.27	86.59
	Overall, Acc. %	98.78	99.52	97.74	98.12

Table 4: The obtained producer's accuracy (PA), user's accuracy (UA), and overall accuracy values for Perth (top) and Muscat (bottom). Values below 90% are highlighted.

Perth	**MAE**	**RMSE**		**Muscat**	**MAE**	**RMSE**
2020	1.74	2.25		2020	7.04	7.26
2015	2.95	3.38		2015	6.38	6.79
2010	6.76	7.08		2011	15.81	16.10
2005	5.93	6.12		2005	8.90	9.23
2000	7.28	7.41		2000	10.30	10.65

Table 5: MAE and RMSE between Landsat and MODIS.

6. Land Use/Land Cover Changes and SUHI Intensity

6.1 Overview of LU/LC Changes in Perth and Muscat

Figure 4 shows the LULC maps for Perth and Muscat in 2020 for visual inspection. More details are provided in Table 6. Table 6 (top) shows the land cover area in Perth from 2000 to 2020, indicating a substantial growth in urban areas, with an increase of 123.6 km², now comprising over half of the land area (51.51%). The industrial areas have also expanded, albeit slower, by 37.52 km². Meanwhile, there is a slight reduction in vegetation and water areas, by 11.01 km² and 8.12 km², respectively. The most significant change is observed in the bare soil category, which decreased by 141.99 km². On the other hand, there has been a noticeable expansion in urban development in Muscat (Table 6, bottom), with the urban area growing by 165.38 km², now representing 10.05% of the land. Industrial zones have seen a more modest increase of 33.78 km². Vegetation cover has

decreased slightly by 2.68 km², and water bodies have also experienced a marginal decline of 2.8 km². The most dramatic change is evident in the bare soil category, which has reduced 207.48 km². These shifts suggest a significant change in land use, possibly attributable to development and urbanization processes.

6.2 Comparison between LST data, NDVI and NDBI

This section involves a comprehensive comparison of LST between Perth and Muscat over a five-year period, employing a tailored approach to applying the *NDVI* to suit each city's specific vegetation characteristics. In Perth, an *NDVI* threshold of 0.3 was utilized to identify densely vegetated areas, and the average LST for these regions was calculated. Conversely, due to Muscat's sparser vegetation, the NDVI threshold was adjusted to 0.2, enabling a more accurate representation of its limited vegetative areas in determining the mean LST.

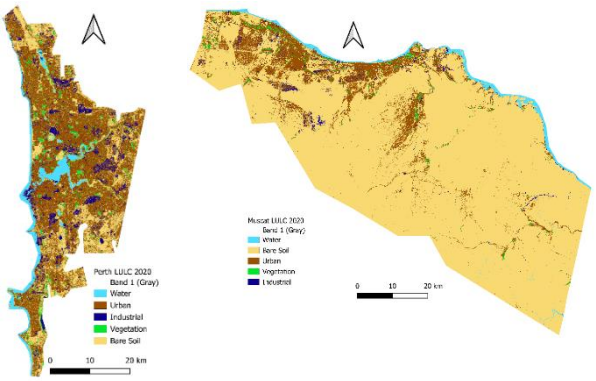

Figure 4: LULC Classes for 2020 for Perth (left) and Muscat (right).

Perth	Km² (%)				
Year	Urban	Industrial	Vegetation	Water	Bare Soil
2020	738.74 (51.51%)	131.63 (9.18%)	63.70 (4.44%)	92.76 (6.47%)	407.32 (28.4%)
2015	727.89 (50.75%)	118.86 (8.29%)	81.49 (5.68%)	89.52 (6.24%)	416.38 (29.03%)
2010	713.96 (49.78%)	102.99 (7.18%)	73.48 (5.12%)	93.71 (6.53 %)	450.01 (31.38%)
2005	676.83 (47.19%)	100.65 (7.02%)	78.25 (5.46%)	92.57 (6.45%)	485.85 (33.88%)
2000	615.14 (42.89%)	94.11 (6.56%)	74.71 (5.21%)	100.88 (7.03%)	549.31 (38.30%)
Change	123.6	37.52	-11.01	-8.12	-141.99

Muscat	Km² (%)				
Year	Urban	Industrial	Vegetation	Water	Bare Soil
2020	311.80 (10.05%)	34.84 (1.12%)	21.96 (0.71%)	56.48 (1.82%)	2678.90 (86.31%)
2015	258.68 (7.34%)	26.93 (0.87%)	17.57 (0.57%)	50.95 (1.64%)	2749.84 (89.6%)
2010	211.01 (6.8%)	15.61 (0.5%)	19.99 (0.64%)	53.27 (1.72%)	2804.10 (90.34%)
2005	178.12 (5.74%)	5.97 (0.19%)	18.13 (0.58%)	49.15 (1.58%)	2852.61 (91.9%)
2000	146.42 (4.72%)	1.06 (0.03%)	26.44 (0.85%)	53.68 (1.73%)	2876.38 (92.67%)
Change	165.38	33.78	-2.68	-2.8	-207.48

Table 6: LU/LC area by class for Perth (top) and Muscat (bottom).

The study also incorporated the NDBI, initially applying a threshold of 0.1 in both cities. However, this threshold in Muscat predominantly indicated areas of bare soil rather than urban zones, a phenomenon attributed to the local geology. The bare soil in Muscat is characterized by sedimentary coarse grey gravel, commonly found in the lowland zone and composed of a mixture of boulders, pebbles, sand, and silt. Also, the highland zone is distinguished by dark lava rocks such as Ophiolite and Gabbro, known for their high thermal conductivity and ability to absorb short-wave radiation (Charabi & Bakhit, 2011). Given these geological considerations, the NDBI threshold for Muscat was refined to include values between 0.0 and 0.1. This adjustment more accurately delineates urban areas than the higher values that indicate bare soil landscapes. Such a modification ensures that the LST calculations for Muscat are based on the urban extent, allowing for a more precise analysis of the SUHI effect in this unique environmental context.

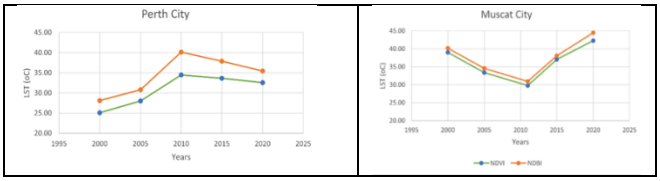

Figure 5: LST, NDVI, and NDBI temporal trends for Perth and Muscat between 2000 and 2020.

Figure 5 illustrates that Perth experienced a gradual increase in LST associated with NDVI and NDBI, with a notable divergence in 2010 where the LST for built-up areas exceeded that for vegetated areas by 5.66°C. Muscat, however, exhibited more pronounced variations, particularly between 2011 and 2020, when the LST for vegetated and built-up areas surged by 12.51°C and 13.49°C, respectively. This indicates a significant shift in urban thermal properties, possibly due to varying urban development and vegetation management practices. The consistently higher LST in urbanized zones compared to vegetated areas underscores the influence of land cover on urban temperatures. Moreover, the relationship among LST, NDBI, and NDVI is noteworthy. A strong positive correlation exists between NDBI and LST, indicating that as urbanization increases, so does the LST. Conversely, a negative correlation is observed between NDVI and LST, suggesting that areas with more vegetation tend to have lower surface temperatures. Additionally, NDBI and NDVI share a significantly negative correlation, underscoring the inverse relationship between urbanization and vegetation cover.

6.3 Correlation analysis between LST and LULC

The data in Table 7 shows that different LULC types have different mean and median LST values, reflecting their thermal properties and heat retention capacities. For example, water and vegetation tend to have lower LST than urban and industrial areas, as they have higher albedo and evapotranspiration rates. In contrast, bare soil has intermediate LST depending on its moisture and mineral content.

The data also shows that urban areas, which include residential, commercial, and mixed-use developments, have higher LST than rural areas. This indicates the presence of SUHI effects in both Perth and Muscat, as urbanization leads to increased surface heating and reduced cooling mechanisms. The difference in LST between urban and rural areas is more pronounced in Muscat than in Perth, as Muscat has a higher degree of urbanization and a lower proportion of green spaces.

Perth	2000				2020		
Class	Mean	Median	Sd		Mean	Median	Sd
Water	20.43	20.52	0.93		22.28	21.79	1.60
Urban	26.44	26.42	1.35		35.15	35.34	1.73
Industrial	25.88	26.28	3.57		34.12	34.58	2.88
Vegetation	25.22	25.37	1.60		32.34	32.48	1.94
Bare Soil	27.21	27.18	2.09		34.80	35.02	2.74
Muscat							
Class	Mean	Median	Sd		Mean	Median	Sd
Water	29.21	28.77	1.79		33.10	32.29	2.26
Urban	41.24	41.07	1.68		45.68	45.99	2.06

Industrial	40.48	39.93	1.59		45.48	46.22	3.05
Vegetation	39.35	39.55	2.21		42.90	43.18	2.67
Bare Soil	40.45	40.69	3.26		45.36	45.75	2.95

Table 7: Comparison of LST Across Different LULC in Perth and Muscat.

It reveals that LST has changed over time in both cities, following urban growth trends and land cover changes. For Perth, the mean LST of urban areas increased from 26.44°C in 2000 to 35.15°C in 2020, while the mean LST of rural areas increased from 24.29°C to 29.81°C in the same period. For Muscat, the mean LST of urban areas increased from 41.24°C in 2000 to 45.68°C in 2020, while the mean LST of rural areas increased from 36.34°C to 40.45°C in the same period. These changes suggest that SUHI intensity has increased in both cities over the past two decades, as urban expansion and land cover transformation have altered the thermal characteristics of the surface.

6.4 Relationship between Land Development Patterns and SUHI Intensity

The resultant SUHI Intensity highlights the extent of Perth's urban heat island effect. It provides insights for urban planning and environmental management strategies to mitigate this phenomenon. Table 8 shows SUHI intensity observed in Perth versus Muscat over the last twenty years, revealing interesting trends that align closely with how each city has developed and used its land. In Perth, the SUHI intensity has steadily increased, from 1.29°C in 2000 to 4.63°C in 2020. This rise in SUHI intensity coincides with the expansion of urban areas, from 42.89% to 51.51% of the land cover, suggesting a strong link between urban development and increased urban temperatures in the city's core compared to surrounding non-urban areas. The growth in industrial areas also mirrors this rise in SUHI, which could be attributed to the additional heat generated by industrial activity.

The land cover data in Muscat reveals a relatively small increase in urban area over the two decades, from 4.72% to 10.05%. The SUHI intensity has remained low and even negative at times, as seen with –0.43°C in 2011 and –0.07°C in 2015. This indicates that in some years, non-urban areas in Muscat were warmer than urban ones. The overwhelming dominance of bare soil, consistently above 86%, along with Muscat's hot climate, could explain the minimal variation in SUHI, as the vast open land absorbs and re-radiates heat similar to urban areas. This is further evidenced by the occasional negative SUHI values, indicating that non-urban areas can be as warm or warmer as urban zones. In hot, arid cities like Muscat with extensive bare soil, urban areas can sometimes exhibit lower surface temperatures than surrounding non-urban areas. The stark contrast in land cover drives this phenomenon: the lack of vegetation and moisture in non-urban regions limits their ability to cool through evapotranspiration, while urban surfaces like buildings can radiate heat more efficiently during the night, leading to potentially cooler temperatures compared to the surrounding arid landscape (Naserikia et al., 2022).
In summary, the data from Table 6 indicates that Perth's increasing urban footprint has resulted in a corresponding rise in SUHI intensity, reflecting the heat-retaining properties of urban infrastructure. In contrast, Muscat's unique environmental conditions and land cover composition result in a less pronounced and more variable SUHI effect. These contrasting patterns highlight the importance of local geographical and climatic factors in shaping the SUHI phenomenon and emphasize the need for tailored urban planning strategies to address the specific challenges of each city's SUHI effect.

Figure 6 presents contrasting urban heat dynamics. In Muscat, the SUHI intensity exhibits an irregular pattern, sometimes registering cooler temperatures in urban spaces compared to their non-urban counterparts. This anomaly could be attributed to the extensive presence of bare soil and Muscat's arid conditions, potentially modulating the urban-rural temperature dichotomy. The high thermal inertia of bare soil could contribute to non-urban areas retaining heat, occasionally exceeding urban temperatures.

	Perth City				Muscat city		
Class/Year	**Urban**	**Non-Urban**	**SUHI**		**Urban**	**Non-Urban**	**SUHI**
2020	34.73	30.1	4.63		45.66	45.08	0.58
2015	36.31	31.94	4.37		39.2	39.27	-0.07
2010	37.69	35.13	2.55		31.81	32.24	-0.43
2005	29.55	27.65	1.9		36.04	35.87	0.17
2000	26.61	25.32	1.29		41.23	40.24	0.99

Table 8: Intensity of the SUHI for Perth (left) and Muscat (right), showing mean LST differences between urban and non-urban areas from 2000 to 2020.

Conversely, Perth's development pattern correlates with rising SUHI intensity, affirming the conventional urban heat island effect where urbanization exacerbates thermal accumulation. The trend indicates urban areas progressively warming over the past two decades, which aligns with the observed expansion of urban land cover. The consistent rise in SUHI in Perth underscores the heat-retaining characteristics of urban infrastructure, marking a stark contrast to Muscat's unique environmental interplay, where such a pattern is not as straightforward.

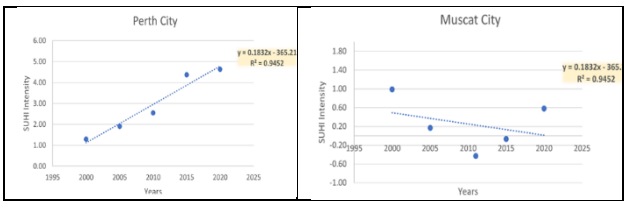

Figure 6: Correlation scatter plot of SUHI intensity trends in Perth (left) and Muscat (right).

Figure 7 contrasting Mean LST with Urban and Non-Urban classifications in Perth and Muscat delineate the influence of land development on thermal patterns. Perth's urban areas consistently register higher temperatures than non-urban zones, affirming the presence of a robust SUHI effect. This divergence suggests urban infrastructure's role in intensifying heat retention. Conversely, Muscat's plot presents a nuanced scenario where urban and non-urban temperatures are comparable, occasionally with urban areas being cooler, reflecting the unique interplay of the city's dry landscape and urban form on its thermal profile.

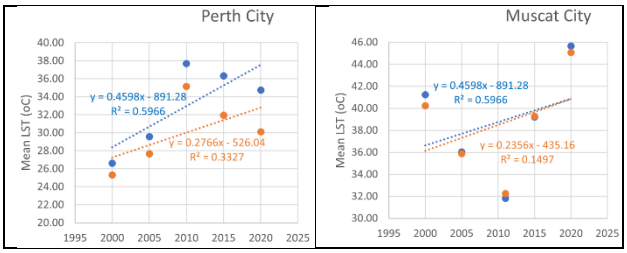

Figure 7: Mean LST with Urban (blue) and Non-Urban (orange) classifications in Perth and Muscat .

The spatial distribution of SUHI in Perth is characterized by a discernible heat intensity pattern aligning with urban development. Contrarily, Muscat exhibits a more uniform thermal landscape with less pronounced heat variation. Temporally, Perth has shown a clear upward trend in SUHI intensity over the years, highlighting an amplification of the surface urban heat island effect that aligns with urban expansion.

Muscat's SUHI intensity fluctuates, reflecting its unique climatic and geographical conditions.

7. Discussion and Conclusion

This study's exploration of SUHI intensity in Perth and Muscat illuminates the profound impact of urbanization on local climatic conditions. A pivotal observation is the correlation between urban land development and increased surface temperatures. The conversion of natural landscapes to urban settings, marked by heat-absorbing materials like concrete, intensifies SUHI effects. This pattern is especially noticeable in rapidly urbanizing regions with diminishing green spaces. Perth and Muscat's contrasting urban profiles exemplify this phenomenon.

Comparing Perth and Muscat offers insights into how different urbanization rates and climatic conditions influence SUHI. In addition to the reasons mentioned in the previous section (different landscape compared with surroundings), there are a few more reasons to take into account. While the population of the Perth metro area duplicated between 2000 and 2025, mainly because of immigration, this number in Muscat has almost tripled. However, this happened in a natural way and, as a consequence, the number of cars in Australia has increased much more in comparison to Oman, and affecting negatively the urban heat. This comparison suggests that urban planning must be context-specific, considering each city's unique environmental and climatic backdrop. Although the study used sound methods and acknowledged constraints, like using particular satellite data and focusing on just two cities, future work could expand its reach by including various urban settings and utilizing more data sources for a deeper understanding of SUHI phenomena.

Future research should not only focus on comparing the impact of “urban” to SUHI but also investigate specific factors driving the observed SUHI intensity, such as land cover types, urban density, and the role of vegetation. It is also planned to compare with other cities and regions to contextualize the findings and better assess the generalizability of the results.

References

Aslan, N., & Koc-San, D. (2021). The Use of Land Cover Indices for Rapid Surface Urban Heat Island Detection from Multi-Temporal Landsat Imageries. ISPRS International Journal of Geo-Information, 10(4), 416.

Bulatov, D., Burkard, E., Ilehag, R., Kottler, B., & Helmholz, P. (2020). From multi-sensor aerial data to thermal and infrared simulation of semantic 3D models: Towards identification of urban heat islands. Infrared Physics & Technology, 105, 103233.

City of Perth. (2015). Greening the City: Perth's Urban Forest Strategy. https://engage.perth.wa.gov.au/urban-forest-plan

Chen, H., Deng, Q., Zhou, Z., Ren, Z., & Shan, X. (2022). Influence of land cover change on spatio-temporal distribution of urban heat island —a case in Wuhan main urban area. Sustainable Cities and Society, 79, 103715.

Charabi, Y., & Bakhit, A. (2011). Assessment of the canopy urban heat island of a coastal arid tropical city: The case of Muscat, Oman1. Atmospheric Research, 101(1-2), 215-227.

Congalton, R. G. (1991). A review of assessing the accuracy of classifications of remotely sensed data. Remote Sensing of Environment, 37(1), 35-46.

Dutta, K., Basu, D., & Agrawal, S. (2019). Nocturnal and diurnal trends of surface urban heat island intensity: A seasonal variability analysis for smart urban planning. ISPRS Annals, IV-5/W2, 25-32.

Fallatah, A., & Imam, A. (2023). Detecting Land Surface Temperature Variations Using Earth Observation at the Holy Sites in Makkah Saudi Arabia. Sustainability, 15(13355).

Grimmond, S. (2007). Urbanization and global environmental change: local effects of urban warming. The Geographical Journal, 173.(1), 83–88.

Karimi, A., Mohammad, P., Gachkar, S., Gachkar, D., García-Martínez, A., Moreno-Rangel, D., & Brown, R. D. (2021). Surface urban heat island assessment of a cold desert city: A case study over the Isfahan metropolitan area of Iran. Atmosphere, 12(10), 1368.

Li, W., Wang, K., Han, G., Wang, H., Tan, N., & Yan, Z. (2022). Integrated diagnosis and time-series sensitivity evaluation of nutrient deficiencies in medicinal plant (Ligusticum chuanxiong Hort.) based on UAV multispectral sensors. Frontiers in Plant Science, 13, 1092610.

Liu, Y., Zhang, Z., Yao, Y., & Lu, H. (2022). Effects of urban built-up area expansion on land surface temperature differences between urban and emerging urban areas in China: 2001–2020. Science of the Total Environment, 821, 153347.

Li, X., Zhou, Y., Asrar, G. R., Imhoff, M., & Li, X. (2017). The surface urban heat island response to urban expansion: A panel analysis for the conterminous United States. Science of the Total Environment, 605–606, 426-435.

Morabito, M., Crisci, A., Guerri, G., Messeri, A., Congedo, L., & Munafò, M. (2021). Surface urban heat islands in Italian metropolitan cities: Tree cover and impervious surface influences. Science of the Total Environment, 751, 142334.

Naserikia, M., Hart, M. A., Nazarian, N., & Bechtel, B. (2022). Background climate modulates the impact of land cover on urban surface temperature- Scientific Reports, 12(1), 15433. https://doi.org/10.1038/s41598-022-19431-x

Nebel, S., & von Richthofen, A. (2016). Urban Oman - Trends and Perspectives of Urbanisation in Muscat Capital Area. November 2016 Edition: HABITAT - INTERNATIONAL: Schriften zur internationalen StadtentwicklungPublisher: LIT Verlag Berlin

Oke, T. R. (1982). The energetic basis of the urban heat island. Quarterly Journal of the Royal Meteorological Society, 108(455), 1-24.

Santamouris, M. (2015). Analyzing the heat island magnitude and characteristics in one hundred Asian and Australian cities and regions. Science of the Total Environment, 512–513, 582–

Shahfahad, Naikoo, M. W., Islam, A. R. M. T., Mallick, J., & Rahman, A. (2022). Land use/land cover change and its impact on surface urban heat island and urban thermal comfort in a metropolitan city. Urban Climate, 41, 101052.

Shastri, H., & Ghosh, S. (2019)2. Urbanisation and surface urban heat island intensity (SUHII)3. In C. Venkataraman, T. Mishra, S. Ghosh, & S. Karmakar (Eds.), Climate change signals and response (pp. 83–99)1. Springer.

Zhang, Y., Odeh, I. O. A., & Han, C. (2009). Bi-temporal characterization of land surface temperature in relation to impervious surface area, NDVI and NDBI, using a sub-pixel image analysis. International Journal of Applied Earth Observation and Geoinformation, 11(4), 256–264.